Available online at www.sciencedirect.com

ScienceDirect

Energy Procedia 137 (2017) 3–13

Energy Procedia

www.elsevier.com/locate/procedia

14th Deep Sea Offshore Wind R&D Conference, EERA DeepWind'2017, 18-20 January 2017, Trondheim, Norway

Design and fatigue analysis of monopile foundations to support the DTU 10 MW offshore wind turbine

Joey Velarde, Erin E. Bachynski

Department of Marine Technology

Norwegian University of Science and Technology, NO-7491 Trondheim, Norway

Abstract

This study aims to investigate the challenges and feasibility of extending monopile technology for larger wind turbines and deeper water.

Preliminary monopile designs to support the DTU 10 MW reference wind turbine were established for water depths 20 m, 30 m, 40 m and 50 m. To properly account for the pile-soil interaction and the rigid pile behavior of large-diameter piles, lateral soil stiffness was derived using the finite element software Plaxis 3D.

To verify the preliminary design, FLS analyses were done using the SIMO-RIFLEX computational tool. As the water depth increases, the contribution of hydrodynamic loads to fatigue damage is found to be larger. A method for predicting total fatigue damage using fewer representative sea states was introduced: a fatigue Damage Parameter (FDP) was established to correlate fatigue damage to environmental condition by means of thrust, significant wave height (Hs) and wave peak period (Tp), and to select representative conditions. Using at least 30% of the total number of conditions resulted in at least 90% accuracy in damage prediction.

Peer-review under responsibility of SINTEF Energi AS.

Keywords: offshore wind energy; monopile; pile-soil interaction; fatigue analysis

1. Introduction

The offshore wind energy market, particularly in Europe, has achieved a rapid growth in the past several years. The offshore wind energy market's growth is related to the European Union's renewable energy policies, which aim for at least 27 % of the final energy consumption from renewable energy sources at the end of 2030 [1]. To reduce the levelized cost of energy of offshore wind farms, larger wind turbines with rated power capacities on the order of 8 MW to 10 MW are being considered.

Larger offshore wind turbines require larger support structures. While monopile foundations still remain the most widely-used support structure due to the relative simplicity of fabrication and installation, several challenges arise

E-mail address: jovl@cowi.com

1876-6102
Peer-review under responsibility of SINTEF Energi AS.
10.1016/j.egypro.2017.10.330

when extending the technology for larger wind turbines and for higher water depths. These include soil-structure interaction, which directly affects the dynamic responses of the structure. In modeling soil-monopile interaction, the current practice follows recommendations from American Petroleum Institute (API) [2]. The method is a Winkler-type approach, which employs uncoupled nonlinear springs represented by p-y curves to support the monopile along the embedded length. The API method is based on testing of two identical steel piles with diameters of approximately 2 meters (or less), and with embedment length to diameter (L/D) ratio of 34.4, while currently installed monopiles have L/D ratio of less than 10 [3,4]. Thus, the API method derived for flexible piles may not be accurate for modeling soil-structure interaction for large-diameter monopiles due to the associated rigid pile behavior. A study on finite element (FE) modeling of large diameter piles by Lesny and Wiemann [5] also showed that the API method tends to overestimate soil stiffness for large diameter monopiles, particularly at greater soil depths. Modeling soil-pile interaction in commercial FE programs, such as PLAXIS and ABAQUS, removes uncertainty associated with the pile behavior being rigid [6].

The design procedure for monopile offshore wind turbines is typically based on design standards from International Electrotechnical Commission (IEC) [7], Det Norske Veritas (DNV) [8] and Germanischer Lloyd (GL) [9]. Extensive load cases must be analyzed in order to check the adequacy of the design with respect to the ultimate limit state (ULS) and fatigue limit state (FLS). The design analysis should consider the dynamic interaction between the wind turbine and support structure, and account for nonlinearities associated with wind turbine control and responses due to aerodynamic and hydrodynamic loading. An integrated analysis tool is therefore required [10]. The resulting stress time series is typically broad-banded as a result of the combination of wind and wave loads, and the fatigue damage is typically estimated using rainflow counting methods with the S-N-curve approach [11]. The computed damage is also known to be sensitive to the wind and wave load modelling [12,13]. The FLS analysis is a time-consuming process and several researchers have suggested methods to reduce computational time [14,15].

In the present work, preliminary monopile designs for water depths 20 m, 30 m, 40 m and 50 m are established to support the DTU 10 MW offshore wind turbine [16]. ULS analysis of these designs, carried out using 1st order and 2nd order wave models applied with Morison's equation, is presented in [17]. The present study focuses on the FLS analysis. The representative design load cases are derived from the long-term wind and wave distribution for Danish central North Sea (Site 15) from the MARINA platform project [18]. A method for predicting fatigue damage using fewer representative sea states is introduced. The accuracy of the procedure, which includes both the selection of representative conditions and damage scaling, is evaluated against fatigue damage calculated using full number of sea states. The proposed procedure could potentially reduce the amount of computational time in fatigue limit state analyses.

The derivation of p-y curves for large diameter piles, wind turbine modeling, preliminary design procedure and selection of fatigue design load cases according to the fatigue damage parameter are described in Section 2. The obtained p-y curves, monopile designs, and results of the fatigue analysis for four different water depths are discussed in Section 3.

2. Methodology

2.1. Pile-Soil FE Model

Plaxis 3D [19] is a three-dimensional finite element program primarily used in the analysis of deformation, stability and groundwater flow in the field of geotechnical engineering. Several advanced constitutive models are available to simulate the non-linear and time-varying soil and/or rock behavior. In this study, the Hardening Soil (HS) model was used. It is an advanced soil model, which uses the following stiffness parameters in estimating soil stiffness: the triaxial loading stiffness (ε_{50}), the triaxial unloading and reloading stiffness (ε_{ur}) and the oedometer loading stiffness (ε_{oed}). In addition, the HS model uses a hyperbolic stress-strain curve which better captures stiffness variation in sand layers compared to other models [21].

Hanssen developed a methodology for extracting soil reaction springs from Plaxis 3D [21]. This approach is valid for a circular pile placed in an arbitrary soil volume. The pile displacements (y-values) are given as default output of node values in Plaxis 3D output program, whereas the corresponding p-values are found by integration of horizontal stresses at the soil-pile interface. The mentioned methodology for extracting the p-values in hollow

cylindrical monopiles involves creating interfaces for both the outer (positive interface) and inner (negative interface) regions of the pile to account for soil-structure interaction on both sides. The general steps in modelling pile-soil interaction include defining the soil properties, defining the pile structure, applying the load, and generating the mesh. The assumed soil properties for a uniform sand layer are summarized in Table 1. For a 30,000 kN applied load, the resulting interface stresses and pile displacement are illustrated in Fig. 1. Note that each applied load corresponds to a single point in the p-y curves. Only the lateral stiffness of the soil represented by the p-y curves was extracted from the FE model, and used as one of the main inputs in modelling and simulation of the monopile foundation.

Table 1: Soil parameters for FE Method using Hardening Soil model

Parameter	Value
Drainage type [−]	Drained
Unit weight unsaturated, γ $[kN/m^3]$	17
Unit weight saturated, γ_{sat} $[kN/m^3]$	20
Secant stiffness in standard drained triaxial test, E_{50}^{ref} $[kN/m^2]$	4.50E+04
Tangent stiffness for primary oedometer loading, E_{oed}^{ref} $[kN/m^2]$	3.75E+04
Unloading and reloading stiffness, E_{ur}^{ref} $[kN/m^2]$	1.20E+05
Power for stress-level dependency of stiffness, m [−]	0.5
Effective Cohesion, c'_{ref} $[kN/m^2]$	1
Effective angle of internal friction, ϕ'_{ref} [°]	36
Angle of dilatancy, ψ [°]	6
Poisson's ratio, ν [−]	0.3

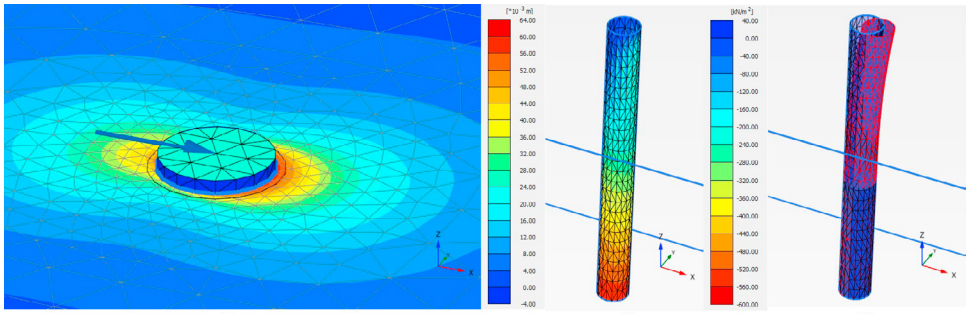

Fig. 1: Graphical stress and displacement calculation
(a) Load application; (b) Stress at the positive interface; (c) pile deflection

2.2. Wind Turbine Model

The DTU 10MW Reference Wind Turbine (DTU 10MW RWT) consists of optimized blades, a drive train and a tower. It was inspired by the NREL 5MW reference wind turbine and was designed for an offshore site (IEC Class 1A). It has a hub height of 119 m relative to the mean seawater level and a rotor diameter of 178.3 m [16].

RIFLEX is a modeling tool developed by MARINTEK for the analysis of flexible marine risers and other slender structures. The program is capable of static, dynamic and eigenvalue analysis based on beam FE modeling. It applies blade element momentum (BEM) theory for aerodynamic load calculation and includes nonlinear soil springs for considering soil-pile interaction [22].

The DTU 10 MW RWT was modeled in RIFLEX as shown in Fig. 2a. The wind turbine blades were modelled using the structural and aerodynamic coefficients from the definition. The tower was modelled as an axisymmetric

pipe having 10 sections of constant diameter each, decreasing from a specified diameter at the bottom to the top of the tower. Similarly, the monopile is modeled in RIFLEX as an axisymmetric pipe. Both tower and monopile have a linearly elastic material with Young's modulus $E = 210\ MPa$ and shear modulus $G = 80.8\ MPa$. The monopile segment below the ground is laterally supported by the nonlinear p-y curves derived from Plaxis 3D for every 2.5 m length. Wind fields were generated using TurbSim, a stochastic and full-field inflow turbulence tool developed by National Renewable Energy Laboratory (NREL) to simulate three-dimensional wind speed vectors in a spatially fixed, two-dimensional vertical rectangular grid [23].

The hydrodynamic loads were based on a 1st order wave model with forces integrated up to the instantaneous undisturbed water line (assuming constant potential (ϕ) above the still water level). Morison's equation was applied with assumed drag (CD) and inertia coefficients (CM) of 0.9 and 2.0, respectively [8].

2.3. Design Procedure

For each water depth, the monopile diameter, thickness and length were established using the RIFLEX models. The monopile thickness was based on the assumed diameter-thickness ratio of 80 [24], while the pile diameter and penetration depth was designed to achieve an overall natural frequency within the soft-stiff region (0.25 Hz) derived from the wind turbine's blade passing frequency intervals, 1P and 3P. For selected penetration depths, the RIFLEX model has to be modified by deriving a set of lateral soil springs from Plaxis 3D. This ensures that the lateral soil stiffness takes into account the complex shift from flexible pile behavior to rigid pile behavior as the embedment length is reduced. Fig. 2b shows the relationship between pile embedment length and natural frequency for a 10 m diameter pile.

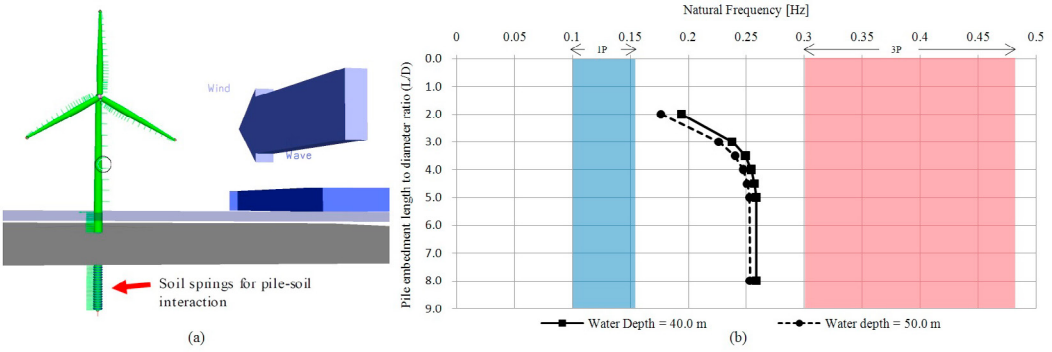

Fig. 2: (a) DTU 10 MW model in RIFLEX; (b) Pile embedment length vs natural frequency for the 10.0 m diameter pile

2.4. Fatigue Limit State Analysis

In the design of offshore wind turbines, fatigue damage assessment is normally done by running an extensive set of design load cases. In this study, a simplified design load case (DLC 1.2) is chosen [7], with co-directional, unidirectional wind and waves, no current, and only operational and below cut-in conditions considered.

For each selected cross section along the monopile, the stress time series was calculated from the time-varying axial force and bending moment obtained in the integrated analysis tool. The point on the upwind direction of the cross section was considered for stress calculation. Stress cycle amplitudes were calculated using the rainflow counting method, and the resulting fatigue damage was calculated based on Palmgren-Miner summation and a representative S-N curve applicable for structures in seawater with cathodic protection [25]. For simplicity, a stress concentration factor of 1.0 was used for fatigue damage calculation.

2.4.1. Environmental Conditions

A number of representative sea states were derived based on long term wind and wave distributions for the selected site. Table 2 summarizes 29 representative conditions arranged by increasing significant wave height. The reduction

of metocean data to only 29 sea states is a significant simplification of real conditions, but allows for relatively efficient preliminary analysis. For fatigue simulations, waves were generated based on JONSWAP spectrum with default peak enhancement factor γ of 3.3 and time step Δt of 0.10 seconds. To avoid unphysical high frequency components, a cut-off frequency ($\omega = \sqrt{2g/H_s}$) was applied to the 1st order wave spectrum [13]. The wind fields (32x32 points, 180 m x 180 m) were generated using TurbSim with a time step Δt of 0.05 seconds. A Kaimal wind spectrum with turbulence according to the normal turbulence model (NTM) for Class A turbines was used, and power law wind shear (with exponent 0.1) was applied [18]. Six 10-minute simulations were carried out for each sea state.

Table 2: Summary of representative sea states from scatter diagram

Sea state	Uw[m/s]	Hs [m]	Tp [s]	Prob.[%]	hrs/year	Sea state	Uw [m/s]	Hs [m]	Tp [s]	Prob. [%]	hrs/year
1	2.2	0.49	5.93	4.8	425	16	17.4	2.58	7.56	2.4	208
2	5.0	0.64	6.06	12.3	1081	17	20.5	2.61	7.58	0.3	30
3	8.0	0.73	6.13	7.5	658	18	11.1	3.21	8.05	0.6	54
4	11.1	0.77	6.17	2.0	176	19	14.3	3.35	8.16	3.7	322
5	14.3	0.80	6.19	0.3	28	20	17.4	3.48	8.26	3.3	291
6	2.2	1.15	6.47	0.3	27	21	20.5	3.55	8.32	0.9	79
7	5.0	1.26	6.55	5.5	483	22	23.6	3.59	8.35	0.1	10
8	8.0	1.43	6.68	16.3	1428	23	14.3	4.21	8.85	0.2	19
9	11.1	1.56	6.78	12.4	1088	24	17.4	4.35	8.96	1.3	113
10	14.3	1.63	6.83	3.7	325	25	20.5	4.47	9.06	1.0	90
11	17.4	1.66	6.86	0.6	52	26	23.6	4.54	9.11	0.2	20
12	20.5	1.69	6.88	0.1	5	27	17.4	5.22	9.68	0.1	7
13	8.0	2.22	7.28	1.8	161	28	20.5	5.36	9.80	0.4	34
14	11.1	2.37	7.40	8.9	778	29	23.6	5.47	9.89	0.2	21
15	14.3	2.51	7.50	8.0	697						
										99.4	8709

2.5. Fatigue Damage Parameter

In this section, a Fatigue Damage Parameter (FDP) is established to correlate fatigue damage of an environmental condition with parameters H_s and T_p. There is no strong correlation between fatigue damage and mean thrust (R^2 = 0.48 for the concept studied here), which removes direct dependence of FDP on thrust or wind speed [17]. The main motivation for establishing an FDP is to quantify how much each environmental condition contributes to fatigue damage and select a number of representative conditions to predict fatigue damage. The proposed approach eliminates the need for running all conditions, thus significantly reducing computation time for FLS.

2.5.1. Formulation

Using Morison's equation, the hydrodynamic force per unit length (F) can be written as the sum of the drag and inertia forces. For inertia-dominated regimes, the drag force contribution can be assumed insignificant:

$$F = \rho C_M A \dot{u}_x \tag{1}$$

where C_M and A are the inertia coefficient and pile cross-sectional area, respectively. The acceleration of the fluid particle in the direction of wave propagation for finite water depth (h) is [26]:

$$\dot{u}_x = \omega^2 \zeta_a \frac{\cosh\left[k(z+h)\right]}{\sinh\left(kh\right)} \cos\left(\omega t - kx\right) \tag{2}$$

By expressing the circular frequency (ω) and wave amplitude ζ_a in terms of wave period (T) and wave height (H), respectively, the bending moment (M) for every section of the monopile due to hydrodynamic load can be expressed in terms of H, T, and moment arm (d):

$$M = d\frac{H}{T^2}\left[\rho C_M A \frac{(2\pi)^2}{2} \frac{\cosh\left[k(z+h)\right]}{\sinh\left(kh\right)} \cos\left(\omega t - kx\right)\right] \tag{3}$$

For monopile foundations supporting a wind turbine, the axial stress is relatively small compared to bending stress. Neglecting the axial force contribution, the sectional stresses can be expressed in terms of bending stress given the moment of inertia (I) and distance from the centroidal axis (y):

$$\sigma = \frac{H}{T^2} C_1, \text{ where } C_1 = d\,\frac{y}{I}\rho C_M A \frac{(2\pi)^2}{2}\frac{\cosh\left[k(z+h)\right]}{\sinh\left(kh\right)}\cos\left(\omega t - kx\right) \tag{4}$$

Assuming that damage accumulates linearly with the number of stress cycles, cycles of constant stress range ($\Delta\sigma$) can be related to the number of cycles to failure (N_f) using Wöhler's equation [27]. The representative S-N curve [25] has two slopes defined by material parameter $m = 3$ and $m = 5$. For FLS analysis, most stress cycle amplitudes lie on the lower region of the S-N curve defined by $m = 5$. Thus, N_f can be expressed as follows:

$$N_f = \bar{a}\left(\Delta\sigma\right)^{-5} \tag{5}$$

where $\log\left(\bar{a}\right)$ refers to the intercept of $\log\left(N\right)$ axis of the S-N curve. The fatigue damage (D) is then predicted using the Palmgren-Miner summation [8]:

$$D = \sum_{i=1}^{n_{cycle}} \frac{n_i(\Delta\sigma_i)}{N_{f,i}(\Delta\sigma_i)}. \tag{6}$$

Assuming a narrow-banded wave frequency spectrum, the actual number of stress cycles (n_i) over a given duration is inversely related to the peak wave period. Using Eqs. 4 and 5, the fatigue damage can be expressed as:

$$D \approx \frac{\left(\frac{1}{T}\right)}{\bar{a}\cdot\left(\Delta\sigma\right)^{-5}} = \frac{H^5\,T^{-11}}{\bar{a}C_1^{-5}}. \tag{7}$$

The formulation assumes fatigue damage is not correlated with mean thrust, wind and wave interaction is insignificant, and that all stress cycles fall at the lower amplitude range defined by the parameter $m = 5$. Using the derived relation for H_s and T_p, and including the probability (P) of each condition to improve selection of representative sea states, the FDP is now defined as in Eq. 8.

$$FDP = H_s^5\,T_p^{-11}P \tag{8}$$

The simplified formulation does not require any prior knowledge about the structure, as opposed to the frequency domain method proposed by Seidel [14].

2.5.2. Procedure

The procedure for calculating the total fatigue damage is illustrated in Fig. 3. A number of representative environmental conditions, out of the total number of conditions in the scatter diagram, shall be selected based on the calculated FDP. The method can be regarded as a variant of importance sampling, where environmental conditions are selected based on estimated fatigue damage contribution.

Given the total number of conditions (M) in the scatter diagram and the number of representative conditions (N), the normalized FDP for each condition (i) and the scale factor (SF) for the total damage can be calculated as in Eqs. 9 and 10.

A simplified fatigue load assessment based on statistical regression models was also presented by Zwick and Muskulus [15], whose performance was demonstrated on a jacket-type foundation under operational conditions. Unlike the FDP method, the proposed method requires calibration of regression parameters for both piecewise linear regression (PLR) and multivariate linear statistical model (LSM).

$$(FDP_{norm})_i = \frac{FDP_i}{\sum_{i=1}^{M}(FDP_i)} \tag{9}$$

$$S_F = \frac{\sum_{i=1}^{M}(FDP_{norm})_i}{\sum_{i=1}^{N}(FDP_{norm})_i}, \text{ where } \sum_{i=1}^{M}(FDP_{norm})_i = 1 \tag{10}$$

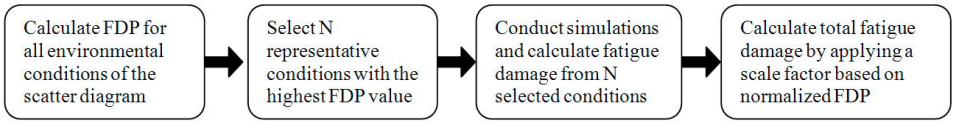

Fig. 3: FDP procedure for calculating fatigue damage

3. Results and Discussion

3.1. P-Y Curves

The derived nonlinear p-y curves for a pile having an 9 m diameter, 110 mm thickness and 35 m embedment for selected shallow depths are shown in Fig. 4. It verifies that the soil stiffness consistently increases with depth up to penetration depths at least twice the pile diameter.

Comparison of derived p-y curves using FE method and API method illustrates good agreement at shallow depths (z = -1.25 m). The API method, however, overestimates soil stiffness with further increase in soil depth due to the linear increase in stiffness whereas the FE method has a parabolic increase. The nonlinear p-y curves derived for all monopile designs are documented in [17].

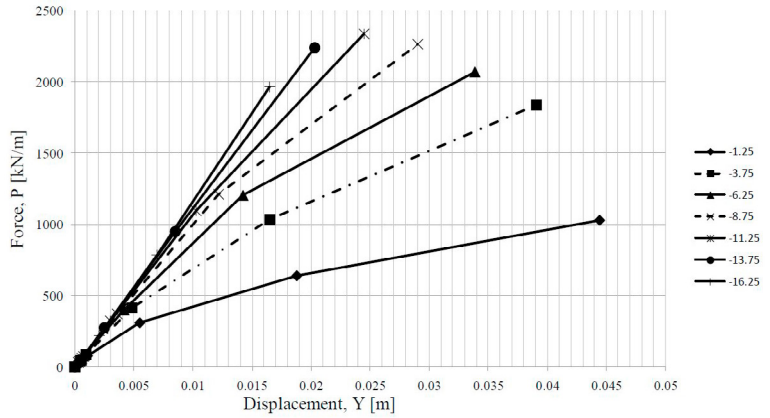

Fig. 4: Extracted p-y curves for the shallow part of the soil [17]

3.2. Preliminary Design

Under extreme load conditions, the stability requirements set for preliminary design include the rotation at mudline not exceeding 0.50° and the lateral deflections at mudline and pile toe not exceeding 120 mm and 20 mm, respectively. The preliminary designs summarized in Table 3 satisfied both yield check and stability requirements, according to static analysis with a combination of rated wind speed and 50-year wave loads and a safety factor of 1.35 [17]. For

each monopile design, the tower diameter and thickness were also increased to achieve a more cost-effective pile design. Note that manufacturing limitations were not considered.

Table 3: Monopile foundation designs

Water depth [m]	Pile diameter [m]	Pile thickness [mm]	Tower *D* scale [-]	Tower thickness scale [-]	Penetration Depth [-]	Natural Frequency [Hz]
20	9	110	1.125	1.25	35	0.251
30	9	110	1.125	1.75	45	0.251
40	10	125	1.25	1	35	0.249
50	10	125	1.25	1.5	45	0.251

The criteria set for foundation stability were evaluated for FE and API method as shown in Table 4. In general, the API method predicted lower deformations. Considering lateral deflections and rotation at seabed, FE method predictions were about 30 % and 19 % higher, respectively. For the lateral deflection at pile toe, a higher deviation was observed for monopiles designed for water depths 30 m and 50 m where the embedment depths were 45 m, which was 10 m higher than that of water depths 20 m and 40 m. This high deviation at higher penetration depth shows that the API method tended to overestimate the soil stiffness with depth. For all water depths, using the API method slightly increased the natural frequency by about 0.01 Hz. Note that the stiffness in the shallow region of the soil, where the two methods showed good agreement, had a more significant influence in the overall static and dynamic response of the structure compared to the deeper part of the soil.

Table 4: Comparison of stability check results between FE method and API method

Water	Lateral deflection at seabed [mm]			Lateral deflection at pile toe [mm]			Rotation at seabed [deg]		
depth [m]	Plaxis	API	Dev. [%]	Plaxis	API	Dev. [%]	Plaxis	API	Dev. [%]
20	33.3	20.7	37.7	-4.9	-4.1	16.9	0.0020	0.0016	20.3
30	52.5	38.3	27.0	-2.7	-1.0	63.3	0.0020	0.0017	16.6
40	87.2	61.5	29.4	-6.4	-6.7	4.5	0.0022	0.0018	21.0
50	101.9	77.5	23.9	-4.0	-2.3	44.1	0.0022	0.0018	17.3

3.3. Fatigue Limit State Analysis

The calculated 20-year fatigue damage for selected points along the monopiles is shown in the outer envelope of Fig. 5, which also shows the relative contribution of each environmental condition. For all water depths, fatigue damage increased from the mean free water level until it reached a maximum value a few meters below the seabed, and then gradually reduced to zero at the end of the pile. The maximum fatigue damage for different water depths and its location are summarized in Table 5. Note that monopile designs for 20 m and 30 m water depths had 9.0 m diameter, while designs for 40 m and 50 m water depths had 10.0 m diameter. Regardless of pile design, the location of maximum fatigue damage fell between 7.0 m and 9.0 m below the seabed. Among the four monopile designs for each water depth, only the design for the 20 m water depth was satisfactory considering FLS. The effect of wave diffraction, however, was not considered. For large diameter piles associated with low Keulegan-Carpenter numbers (inertia-dominated regime), diffraction could potentially reduce the wave load magnitudes, and thus the total fatigue damage. Fig. 5 also shows that, for the 20 m water depth, a larger part of the fatigue damage was given by lower sea states. As water depth increased, the contribution from higher sea states became larger. This implies that hydrodynamic loads become more significant with higher depths.

Table 5: Location of maximum fatigue damage

Water Depth [m]	Maximum fatigue damage	Node	Elevation from mudline [m]
20	0.35	28	-8.75
30	1.27	36	-6.25
40	1.45	48	-8.75
50	6	57	-7.5

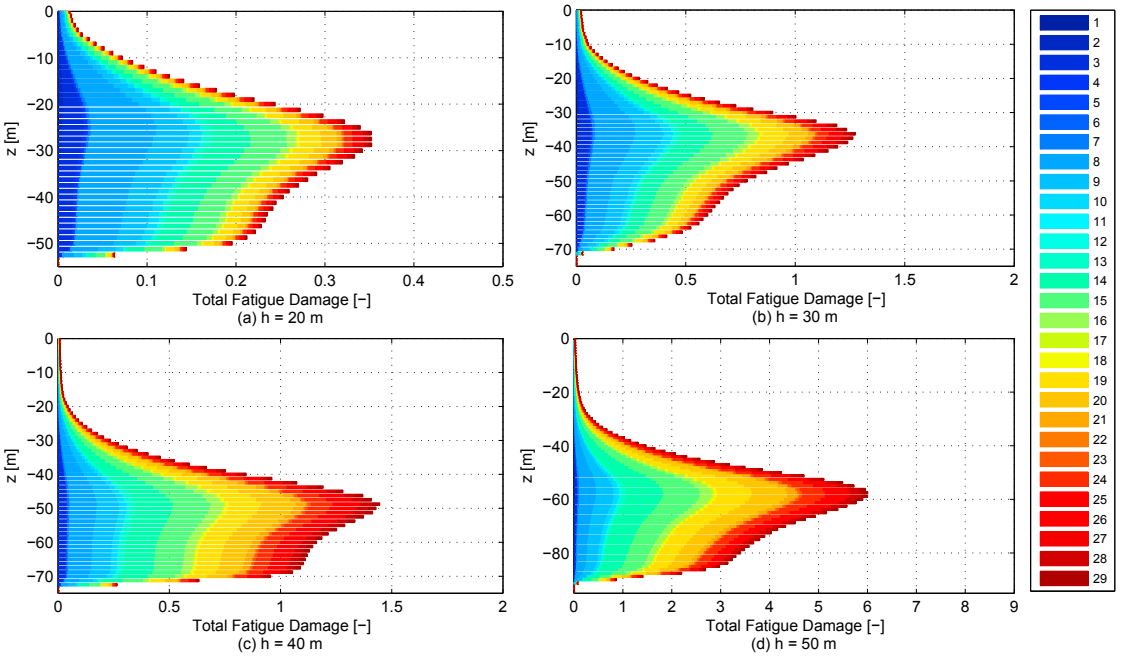

Fig. 5: Total fatigue damage, showing contributions from each environmental condition.

3.4. Fatigue Damage Parameter

3.4.1. Selection of sea states

The representative sea states were selected based on normalized FDP, as illustrated in Fig. 6a. Since FDP only depends on the environmental condition, the selection of sea states is independent of both water depth and structural design.

3.4.2. Results

The calculated fatigue damage for different numbers of representative conditions (N = 3, 9, 15, 20, 26) out of 29 sea states is shown in Fig. 7, with the black line indicating prediction using all 29 sea states. The fatigue predictions from FDP approach are generally underestimated, but demonstrate good prediction if the number of conditions used is at least 30% of the total number of conditions. The number of conditions ($N = 3, 9, 15, 20, 26$) was simply chosen to demonstrate the accuracy of method with respect to increasing the percentage of samples, (i.e. 10%, 30%, 50%, 70%, 90% of the 29 sea states). Based on the FDP shown in Fig. 6a, for $N = 3$, representative sea states 14, 15 and 19 are used. Since they have the highest contribution, these three sea states are also included for all larger values of N.

The accuracy of damage prediction at the section where maximum fatigue damage occurs is shown in Fig. 6b. Using a larger number of representative conditions generally increased the accuracy of prediction, and the method was more accurate for higher water depths. Using at least 30% of the total number of conditions resulted in at least

90% accuracy, but increasing the number of representative conditions from 30% to 70% did not result in a significant increase in accuracy, particularly for water depths 20 m and 30 m.

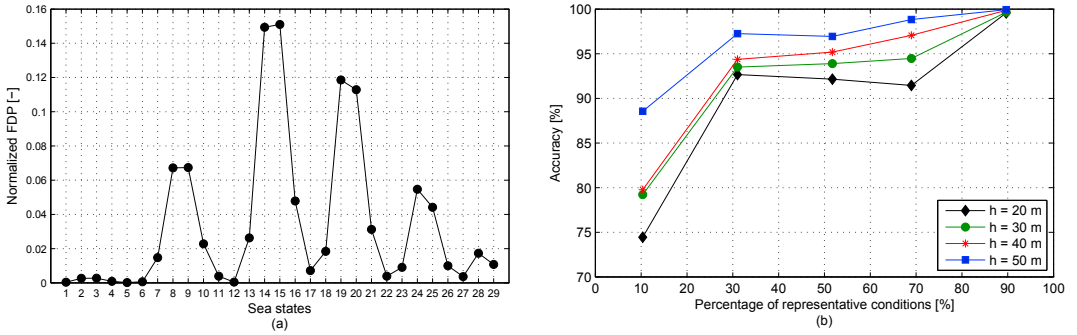

Fig. 6: (a) Normalized FDP for selection of representative sea states; (b) Method accuracy at location of maximum damage

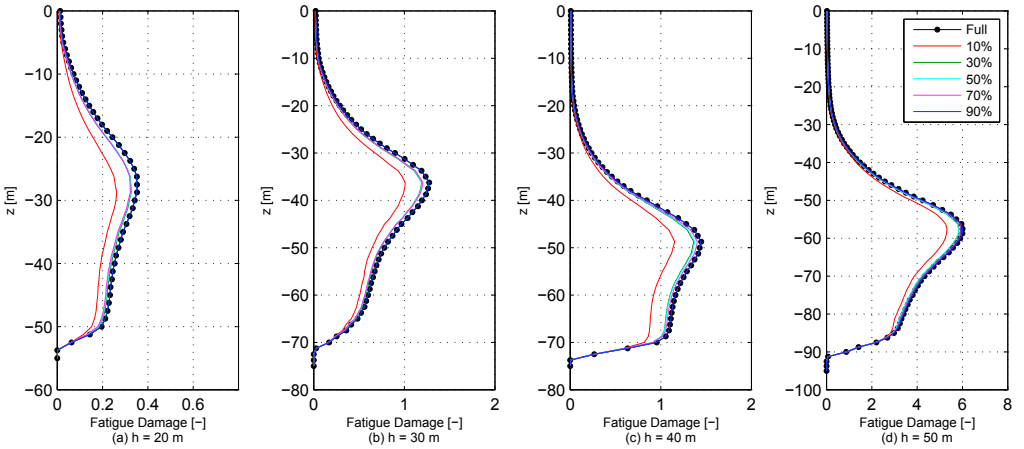

Fig. 7: Fatigue damage prediction for various N representative conditions

4. Concluding Remarks

Preliminary monopile designs for water depths 20 m, 30 m, 40 m and 50 m were established using nonlinear p-y curves derived from FE method. The sensitivity of structural stability with soil lateral stiffness was investigated by comparing the API method with FE method. To verify adequacy of the design, coupled fatigue limit state analyses during operational conditions were conducted using irregular 1st order waves applied with Morison's equation.

Results showed that using API method slightly increased the overall natural frequency of the structure by 0.01 Hz, but tended to underestimate stability requirements. FE method predictions for lateral deflections and rotation at seabed were about 30% and 19% higher, respectively. For lateral deflection at pile toe, the difference in prediction varied depending on the pile diameter and penetration depth.

Fatigue analysis showed that damage contribution from higher sea states increased with water depth, implying that hydrodynamic loads became more significant when designing monopiles for higher water depths. To achieve a more accurate damage prediction, time-domain simulations accounting for the effect of wave diffraction for large monopiles should be carried out.

The FDP procedure for calculating fatigue damage was introduced. Using at least 30% of the total number of conditions resulted in at least 90% accuracy. Further work includes investigation of the applicability of the FDP

procedure with other types of support structures, other (more extensive) site-specific environmental conditions and sensitivity to lumping of environmental conditions.

5. Acknowledgement

Joey Velarde acknowledges support from the European Commission through the Erasmus Mundus European Wind Energy Master (EWEM) Program. The authors also wish to acknowledge the financial support from Research Council of Norway through Center for Ships and Ocean Structures (CeSOS) and Centre for Autonomous Marine Operations and Systems (AMOS, RCN Project number 223254). Thanks are extended to Dr. Stian Baardsgaard Hanssen, Prof. Gudmund Reidar Eiksund, Asst. Prof. Eliz-Mari Lourens and Prof. Andrei Metrikine for stimulating discussions.

References

[1] European Wind Energy Association. Wind energy scenarios for 2030. Technical report, European Wind Energy Association (EWEA); 2015.
[2] American Petroleum Institute. Recommended Practice for Planning, Designing and Constructing Fixed Offshore Platforms - Working Stress Design; 2000.
[3] Krolis VD, van der Zwaag GL, de Vries W. Determining the Embedded Pile Length for Large-Diameter Monopiles. Marine Technology Society Journal; 2010.p. 24-31.
[4] Sørensen SPH, Brødbæk KT, Møller M. Evaluation of Load-Displacement Relationships for Large-Diameter Piles. Faculties of Engineering, Science and Medicine, Aalborg University; 2009.
[5] Lesny K, Wiemann J. Finite-Element-Modelling of Large Diameter Monopiles for Offshore Wind Energy Converters; 2006. p. 1-6.
[6] Augustesen A.H., et al. Numerical modelling of large-diameter steel piles at Horns Rev. Proceedings of the 12th International Conference on Civil, Structural and Environmental Engineering Computing; 2009.
[7] International Electrotechnical Commission. Wind turbines: Part 3: Design requirements for offshore wind turbines; 2009. IEC61400-3.
[8] Det Norske Veritas. Design of Offshore Wind Turbine Structures. Technical Report, DNV; 2014. DNV-OS-J101.
[9] Germanischer Lloyd. Guideline for the Certification of Offshore Wind Turbines; 2012, GL.
[10] Soares, C.G. and Garbatov, Y. Offshore Renewable Energy (ISSC Committee V.4). Ships and Offshore Structures XIX; 2015
[11] Dong, W., Moan, T., and Gao, Z. Long-term fatigue analysis of multi-planar tubular joints for jacket-type offshore wind turbine in time domain. Engineering Structures 2011; 33(6): 2002-2014.
[12] Veldkamp, H.F. and van der Tempel, J. Influence of Wave Modelling on the Prediction of Fatigue for Offshore Wind Turbines. Wind Energy 2005; 8:49-65.
[13] Bachynski EE and Ormberg, H. Hydrodynamic Modeling of large-diameter bottom-fixed offshore wind turbines. ASME 2015 34th International Conference on Ocean, Offshore and Arctic Engineering; St. John's, NL, Canada, 2015.
[14] Seidel M. Wave induced fatigue loads. Stahlbau 83.8: 535-541; 2014
[15] Zwick D, Muskulus M. Simplified fatigue load assessment in offshore wind turbine fatigue analysis. Wind Energy, Wiley Online Library, 19, 265-278; 2016;
[16] Bak C, Zahle F, Bitsche R, Kim T, Yde A, Henriksen LC, Andersen PB, Natarajan A, Hansen MH. Design and performance of a 10 MW wind turbine. DTU Wind Energy Report; 2013.
[17] Velarde J. Design of Monopile Foundations to Support the DTU 10 MW Offshore Wind Turbine. Norwegian University of Science and Technology, Trondheim, Norway; 2016.
[18] Li L, Gao Z, Moan T. Joint Environmental Data at Five European Offshore Sites for Design of Combined Wind and Wave Energy Concepts. ASME 2013 32nd International Conference on Ocean, Offshore and Arctic Engineering; Nantes, France, 2013.
[19] PLAXIS. PLAXIS 2015, The Netherlands; 2015.
[20] PLAXIS. Material Models Manual; 2015.
[21] Hanssen SB. Response of laterally loaded monopiles, PhD Thesis. Norwegian University of Science and Technology, Trondheim, Norway. 2016:226, ISBN 978-82-326-1791-3.
[22] Ormberg H, Bachynski EE. Global analysis of floating wind turbines: Code development, model sensitivity and benchmark study. In: The 22nd International Ocean and Polar Engineering Conference. Rhodes, Greece: International Society of Offshore and Polar Engineers; 2012.
[23] Kelley ND, Jonkman BJ. Overview of the TurbSim Stochastic Inflow Turbulence Simulator. Technical Report, National Renewable Energy Laboratory; 2007.NREL/TP-500-41137.
[24] Offshore Engineering Section, Faculty of Civil Engineering and Geosciences. Monopile Design - Part I, Lecture Notes on Offshore Wind Support Structures (OE5665). Delft University of Technology; 2015.
[25] Det Norske Veritas. Fatigue design of offshore steel structures. Technical Report, DNV; 2012. DNV-RP-C203.
[26] Faltinsen OM. Sea loads on ships and offshore structures. Cambridge University Press; 1998.
[27] Yeter B, Garbatov Y, Guedes Soares C. Fatigue damage assessment of fixed offshore wind turbine tripod support structures. Centre for Marine Technology and Ocean Engineering (CENTEC), Instituto Superior Tcnico, Universidade de Lisboa; 2015.